nature astronomy

LETTERS

https://doi.org/10.1038/s41550-017-0374-z

# Atmospheric reconnaissance of the habitable-zone Earth-sized planets orbiting TRAPPIST-1

Julien de Wit[1*], Hannah R. Wakeford[2,3], Nikole K. Lewis[3], Laetitia Delrez[4], Michaël Gillon[5], Frank Selsis[6], Jérémy Leconte[6], Brice-Olivier Demory[7], Emeline Bolmont[8], Vincent Bourrier[9], Adam J. Burgasser[10], Simon Grimm[7], Emmanuël Jehin[5], Susan M. Lederer[11], James E. Owen[12], Vlada Stamenković[13,14] and Amaury H. M. J. Triaud[15]

**Seven temperate Earth-sized exoplanets readily amenable for atmospheric studies transit the nearby ultracool dwarf star TRAPPIST-1 (refs [1,2]). Their atmospheric regime is unknown and could range from extended primordial hydrogen-dominated to depleted atmospheres[3–6]. Hydrogen in particular is a powerful greenhouse gas that may prevent the habitability of inner planets while enabling the habitability of outer ones[6–8]. An atmosphere largely dominated by hydrogen, if cloud-free, should yield prominent spectroscopic signatures in the near-infrared detectable during transits. Observations of the innermost planets have ruled out such signatures[9]. However, the outermost planets are more likely to have sustained such a Neptune-like atmosphere[10,11]. Here, we report observations for the four planets within or near the system's habitable zone, the circumstellar region where liquid water could exist on a planetary surface[12–14]. These planets do not exhibit prominent spectroscopic signatures at near-infrared wavelengths either, which rules out cloud-free hydrogen-dominated atmospheres for TRAPPIST-1 d, e and f, with significance of 8σ, 6σ and 4σ, respectively. Such an atmosphere is instead not excluded for planet g. As high-altitude clouds and hazes are not expected in hydrogen-dominated atmospheres around planets with such insolation[15,16], these observations further support their terrestrial and potentially habitable nature.**

We observed transits of TRAPPIST-1 planets d, e, f and g with four visits of the Hubble Space Telescope (HST). Each of the visits contained two planetary transits (Fig. 1), planets d and f in visit 1 (4 December 2016) and visit 3 (9 January 2017), and planets e and g in visit 2 (29 December 2016) and visit 4 (10 January 2017). The observations were conducted using the forward scanning mode with the near-infrared (1.1–1.7 μm) G141 grism on the Wide Field Camera 3 (WFC3) instrument (see Methods). We capitalized on the frequency of the transit events in the TRAPPIST-1 system to select observation windows encompassing transits from two different planets, thereby optimizing the time allocation. The time sensitivity of these observations (TRAPPIST-1's visibility window closing in January 2017) combined with our multiple-transit-per-visit approach constrained us to perform exposures when the HST crossed through the South Atlantic Anomaly (SAA).

Visits 1, 3 and 4 contained SAA crossing events that forced the HST into GYRO mode, where its fine-pointing ability was lost. The loss of fine pointing during and following the SAA crossing events caused the spectral position on the detector to change over time. In addition, during the SAA crossing, a greater number of cosmic ray hits were introduced to the observations/exposures. We used the Intermediate MultiAccum output files from the CalWF3 pipeline and corrected for this by cross-correlating each spectral reading in the individual exposures and interpolating (see Methods). The raw light curves present primarily ramp-like systematics on the scale of HST orbit-induced instrumental settling discussed in previous WFC3 studies[17–19] (Fig. 1). We chose here to not discard the first orbit of each visit, which is affected by larger systematics, but rather to develop a holistic systematic model allowing us to account for the time-dependent effects observed across the orbits of a visit[19,20], to prevent reducing the observation baseline (see Methods).

Despite the SAA crossing events in three of our visits, we mostly achieved per-orbit/visit precisions on a par with that achieved for the 4 May 2016 observations of planets b and c. Summing over the entire WFC3 spectral range, we derived a white light curve across the WFC3/G141 bandpass and reached an averaged standard deviation of the normalized residuals (SDNR) of 220 ppm over 21 of the 23 orbits (two orbits were heavily affected by the SAA crossing; see Methods), which is 1.5 times the photon noise limit. We reduced, corrected for instrumental systematics and analysed the data using independent methods presented in previous studies[9,19,21,22]. The independent analyses conducted by subgroups of our team yield consistent results, which we report below.

We first analysed the white light curves to measure transit depths and timings for comparison with previous observations. In retrieving these parameters, we treated each visit separately and simultaneously fitted for the two transits in each visit while accounting for instrumental systematics following ref. [9]. Due to the reduced phase coverage of HST observations, we fixed the system's parameters to the values reported in the literature[1] while estimating the transit

[1]Department of Earth, Atmospheric and Planetary Sciences, Massachusetts Institute of Technology, Cambridge, MA, USA. [2]Astrophysics Group, University of Exeter, Devon, UK. [3]Space Telescope Science Institute, Baltimore, MD, USA. [4]Astrophysics Group, Cavendish Laboratory, Cambridge, UK. [5]Space sciences, Technologies and Astrophysics Research (STAR) Institute, Université de Liège, Liege, Belgium. [6]Laboratoire d'astrophysique de Bordeaux, Univ. Bordeaux, CNRS, Pessac, France. [7]University of Bern, Center for Space and Habitability, Bern, Switzerland. [8]Astrophysics Division of CEA de Saclay, Gif-sur-Yvette, France. [9]Observatoire de l'Université de Genève, Sauverny, Switzerland. [10]Center for Astrophysics and Space Science, University of California, San Diego, La Jolla, CA, USA. [11]NASA Johnson Space Center, Houston, TX, USA. [12]Astrophysics Group, Imperial College London, Blackett Laboratory, London, UK. [13]Jet Propulsion Laboratory, California Institute of Technology, Pasadena, CA, USA. [14]Division of Geological and Planetary Sciences, California Institute of Technology, Pasadena, CA, USA. [15]School of Physics and Astronomy, University of Birmingham, Birmingham, UK. Julien de Wit, Hannah R. Wakeford and Nikole K. Lewis contributed equally to this work. *e-mail: jdewit@mit.edu

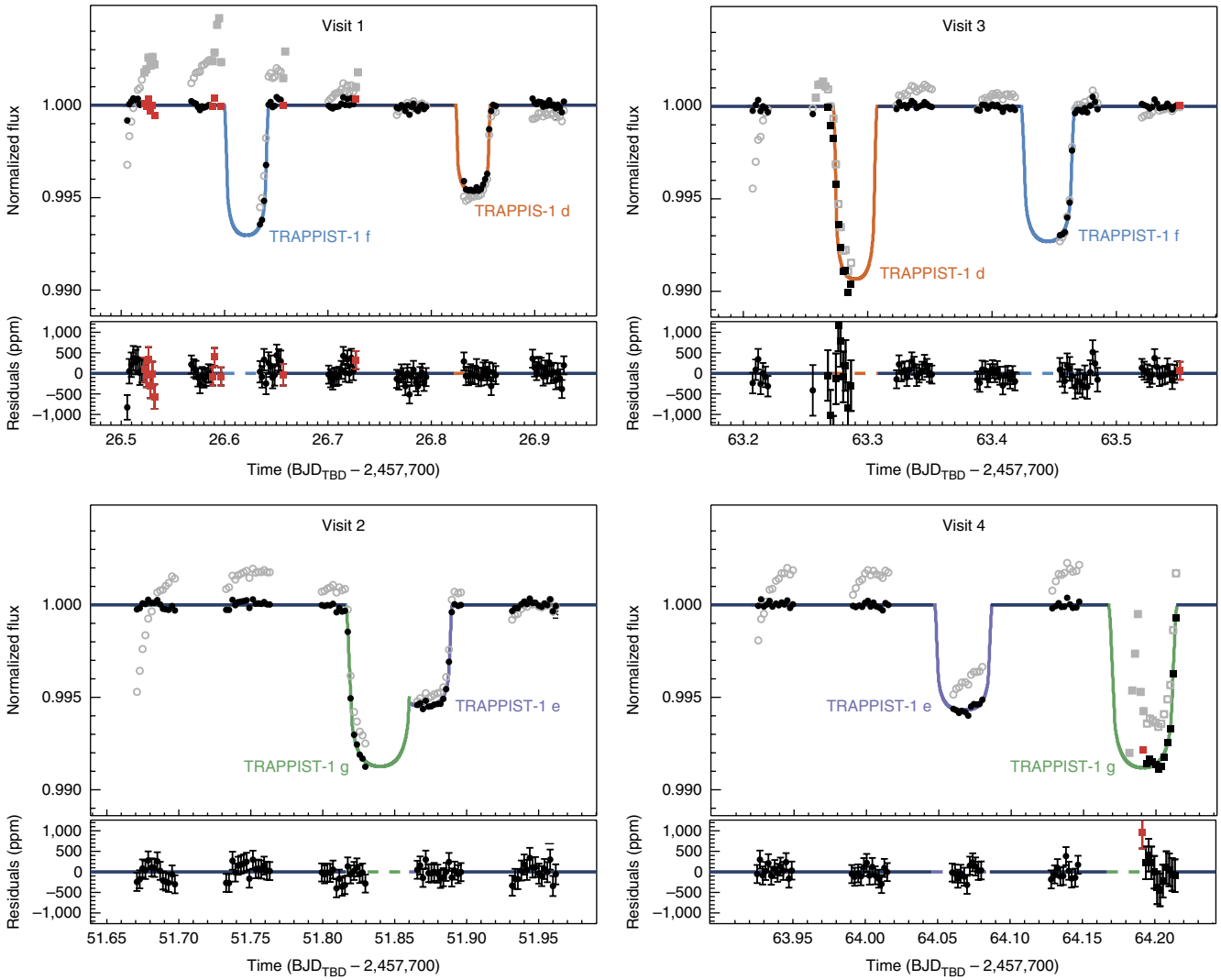


**Fig. 1 | Hubble/WFC3 white light curves of the four TRAPPIST-1 habitable-zone planets d, e, f and g over four visits.** In the top panel of each visit, the raw normalized light curves (grey) are shown with the systematic corrected light curves (black) against the best-fit transit model (coloured solid line). In visits 1, 3 and 4, the observations were taken during the SAA crossing indicated by filled grey points in the raw data and red points in the corrected data. During and following the SAA crossing, the HST entered GYRO mode, and we show each of these impacted exposures as squares in the datasets. The bottom panel of each visit shows the best-fit residuals with their 1σ error bars. We again indicate where the SAA and gyro-mode exposures occurred during each visit, and the dashed horizontal lines indicate where the transit occurred. Time is measured in barycentric Julian date/barycentric dynamical time (BJD$_{TBD}$) – 2,457,000.

times and depths. However, we let the band-integrated limb-darkening coefficients[9] and the orbital inclinations[1] float under the control of priors, to propagate their uncertainties on the transit depth and time estimates with which they may be correlated. We report the transit depth and time of transit centre estimates in Table 1. The transit depth of planet d during visit 3 was poorly constrained and substantially affected by a spectral drift 20 pixels long over the detector due to the SAA crossing at the beginning of the orbit covering this transit. Although the effect of the SAA crossing, and that of the resulting GYRO mode, can be corrected if the crossing occurs either during an orbit or at its end, they cannot be corrected with high precision if the crossing occurs at the beginning of an orbit. Apart from this transit depth, all others are in agreement within 2σ with the values reported in the literature[1]. We reach a precision of ~40 s on the transit timings for all but the transit of planet e during visit 4, for which neither the ingress nor the egress of the planet's transit is recorded.

We then analysed the light curves in ten spectroscopic channels (1.15–1.65 μm), fitting for wavelength-dependent transit depths, instrumental systematics and stellar baseline levels. We used the wavelength-dependent priors on the limb-darkening coefficients reported in ref. [9]. Our pipelines lead to an average SDNR of 520 ppm per 112 s exposure (see Methods) on the spectrophotometric time series split into ten channels (resolution $\lambda/\Delta\lambda$, where $\lambda$ is wavelength, is asymptotically equal to 33). We derived the transmission spectra of planets e and f jointly from visits 2 and 4 and visits 1 and 3, respectively. Due to increased scatter and cosmic ray hits during the SAA passes, we were unable to derive a transmission spectrum from visit 3 for planet d and visit 4 for planet g, and thus used only visit 1 and visit 2, respectively. The resulting transmission spectra are shown in Fig. 2.

The individual transmission spectra show no significant features. A comparison with aerosol-free versions of hydrogen-dominated atmospheres like those of the Solar System giant planets allows us to rule out such atmospheres at 8σ, 6σ and 4σ for TRAPPIST-1 d, e and f, respectively. The current data result in only a 2σ confidence level for planet g, which is not significant enough to rule out this scenario for the planet. As for planets b and c (ref. [9]), many

**Table 1 | Transit depths and timings of TRAPPIST-1 planets d, e, f and g from programme HST-GO-14873**

| | | TRAPPIST-1 d | TRAPPIST-1 e | TRAPPIST-1 f | TRAPPIST-1 g |
|---|---|---|---|---|---|
| Visit 1 (4 December 2016) | Transit depth[a] | 3,984 ± 87 | - | 6,227 ± 192 | - |
| | Transit timing[b] | 726.84005 ± 0.00041 | - | 726.62108 ± 0.00048 | - |
| Visit 2 (29 December 2016) | Transit depth[a] | - | 4,754 ± 88 | - | 7,823 ± 133 |
| | Transit timing[b] | - | 751.87016 ± 0.00036 | - | 751.83978 ± 0.00047 |
| Visit 3 (9 January 2017) | Transit depth[a] | 8,066 ± 354[c] | - | 6,452 ± 172 | - |
| | Transit timing[b] | 763.28978 ± 0.00055[c] | - | 763.44484 ± 0.00049 | - |
| Visit 4 (10 January 2017) | Transit depth[a] | - | 5,005 ± 101 | - | 7,739 ± 219[c] |
| | Transit timing[b] | - | 764.06713 ± 0.00176 | - | 764.19120 ± 0.00061[c] |

Errors are standard deviations derived from the posterior probability distributions from our Markov chain Monte Carlo simulations.[a]Transit depths are reported as part per million (ppm).[b]Timings are reported as barycentric Julian date/barycentric dynamical time − 2,457,000.[c]The transits of planets d and g during visits 3 and 4, respectively, were discarded due to strong systematics induced by a large drift of the stellar spectrum (see Methods).

alternative atmospheric scenarios are consistent with the data, such as atmospheres dominated by water, nitrogen or carbon dioxide (shown, respectively, in blue, dark green and light green in Fig. 2), tenuous atmospheres composed of a variety of chemical species[3–6,23] and atmospheres dominated by aerosols[16]. The consistency of HST/WFC3's transit depth estimates with those of the Spitzer Space Telescope's Infrared Array Camera at 4.5 μm (ref. [1]) implies a lack of significant absorption features between the two different spectral ranges covered[24], thereby further indicating the absence of clear hydrogen-dominated atmospheres.

Hydrogen is a powerful greenhouse gas, and its presence in substantial amounts in an atmosphere therefore affects a planet's habitability. The predominance of atmospheric hydrogen shapes the inner and outer edge of the habitable zone[6,8], the circumstellar region where water could stay liquid on a planetary surface[12–14]. While a substantial amount of hydrogen could prevent the atmospheres of TRAPPIST-1's outer planets to freeze, it would lead to high surface temperatures and pressures for the inner planets that are incompatible with liquid water. To be habitable, the inner planets must therefore have lost most of their atmospheric hydrogen, or never accreted or outgassed important amounts of hydrogen in the first place[6].

Given the irradiation levels experienced by the Earth-sized planets in TRAPPIST-1's habitable zone, theory suggests that the

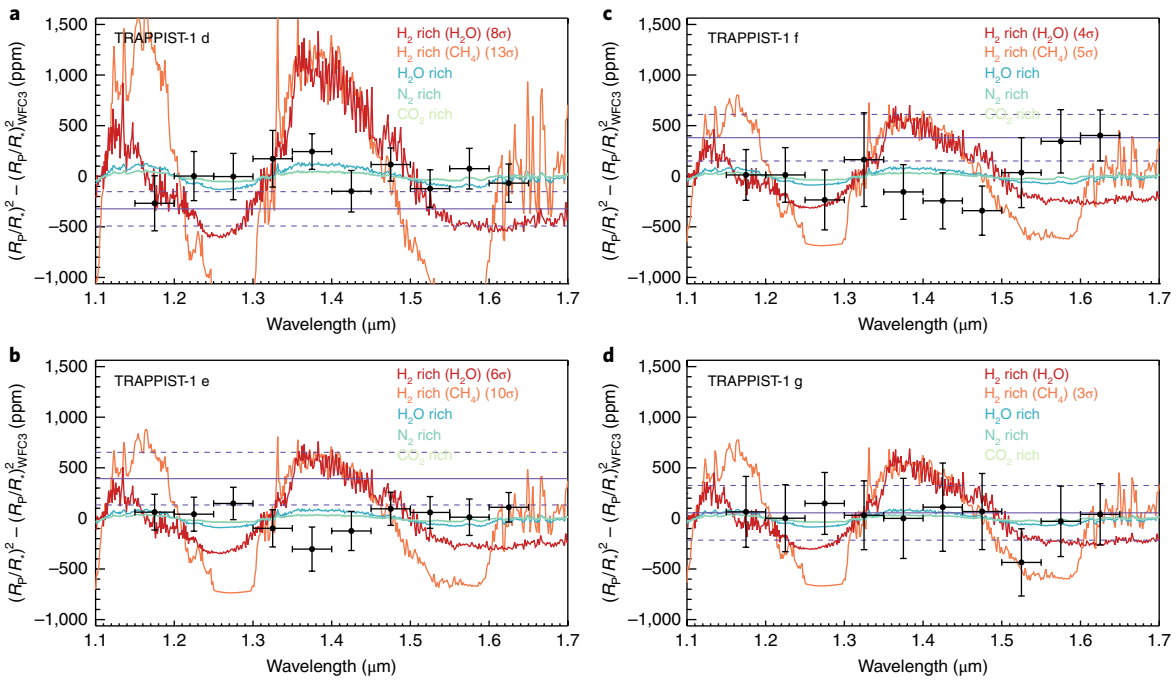


**Fig. 2 | Transmission spectra of TRAPPIST-1 d, e, f and g compared with synthetic atmospheres dominated by hydrogen ($H_2$), water ($H_2O$), carbon dioxide ($CO_2$) and nitrogen ($N_2$).** Trace gases are given in parentheses following the dominant gas. HST/WFC3 measurements are shown as black circles with 1σ error bars. Each spectrum is shown shifted by its average over the WFC3 band. The measurements are inconsistent with the presence of a cloud-free $H_2$-dominated atmosphere at greater than 3σ confidence for planets d, e and f (only the values larger than 3σ are reported in the legends). The measurements for all four planets are consistent with the multiple scenarios of compact atmospheres explored and with the transit depths obtained with the Spitzer Space Telescope's Infrared Array Camera at 4.5 μm (ref. [1]) (solid purple line with 1σ errors shown as dashed lines). $R_P$, apparent planetary radius.

probability of forming aerosols in a hydrogen-rich atmosphere at the pressures probed by the transmission observations presented here is low[15,16]. If exact, aerosol formation theories thus allow us to conclude that TRAPPIST-1 d, e, f and g do not harbour a hydrogen-dominated atmosphere and are terrestrial and potentially habitable.

The next milestone in the characterization of the TRAPPIST-1 planet atmospheres requires spectroscopic measurements that will enable the identification of aerosols (via, for example, attenuation signatures in the planets' transmission spectra[25]) and atmospheres with larger mean molecular masses. This milestone will be possible with the next generation of observatories[2,26,27], notably the James Webb Space Telescope.

As the exploration of habitable-zone and temperate exoplanet atmospheres is initiated over the next decade, a new light will be progressively shone on the concept of the habitable zone. This important concept is currently poorly constrained because its dependence on key parameters such as the host star type and the planets' orbital configuration (including tidal locking) have not been mapped with the current sample at hand, namely the Solar System planets. New perspectives from configurations vastly different from those found in the Solar System will therefore be pivotal to improve our understanding of a planet's habitability and refine the concept of the habitable zone[28].

## Methods

**HST/WFC3 observations.** We observed the transits of TRAPPIST-1 d, e, f and g over the course of four visits, composed, respectively, of 7, 5, 6 and 5 orbits, each containing two of the planetary transits. Visits 1 and 3 contain the transits of planets d and f. Visits 2 and 4 contain the transits of planets e and g. Observations were conducted using the HST/WFC3 near-infrared G141 grism (1.1–1.7 μm) in forward spatial scanning mode[29], which leads to fewer instrumental systematics and should be favoured for faint targets[9,18,30]. Scans in each visit were conducted at a rate of ~0.232 pixels per second, with a final spatial scan covering ~26 pixels (3.38″) in the cross-dispersion direction on the detector.

Visits 1, 3 and 4 contain observations conducted as the HST crossed the SAA. During the SAA, the HST enters GYRO mode and loses its fine-pointing ability. (We flagged manually each frame acquired during the SAA or in GYRO mode because the relevant keywords in the file headers were not updated for each exposure.) In GYRO mode, the stellar spectrum may drift substantially across the detector array between exposures and even during the course of a single spatial scan. This results in a slanted spectral trace across the scan and detector for these affected exposures (Supplementary Fig. 1). The shift caused in each exposure can be measured by cross-correlating the one-dimensional spectrum from each reading of the exposure to a template spectrum (Supplementary Fig. 2), which is used to calculate the relative shift in pixel position in the dispersion direction across the detector for each reading in each exposure for each visit (Supplementary Fig. 3). In visit 2, where no gyro-mode exposures were taken, no pixel level shifts were measured between the successive readings or exposures. During visit 1, the HST entered the SAA four times part of the way into each of the first four orbits, which left the HST in GYRO mode for the rest of these orbits. In visits 3 and 4, the HST crossed the SAA once at the start of an orbit (orbit 2 of visit 3 and orbit 5 of visit 4), which resulted in the GYRO mode being used for the whole orbit, causing substantial shifts in the spectral position over the course of the observation sequences. These orbits were not fully recoverable; avoiding the initiation of orbits coinciding with a planetary transit in the SAA is the only caveat of the observational strategy used here.

To correct for this shift in the spectrum, we use a spline interpolation to realign each of the successive readings for each exposure to a template spectrum, which is made from the zeroth reading of the final exposure. Each of the exposure readings are then aligned such that the pixel column can be summed to produce the total flux over the whole exposure in the related 4.6 nm bin. During the SAA crossing, the exposures are subject to many times more cosmic ray hits than an average observation (Supplementary Fig. 1). During the extraction, we correct for cosmic ray hits in two ways, first spatially by using the surrounding pixels in each two-dimensional reading to use the median to replace the cosmic ray hits, and second after realigning the extracted spectra by using the time axis comparing each pixel in the surrounding exposures and removing the detected cosmic rays. Over the observations, an average of 0.12% of the pixels are corrected for cosmic ray hits.

**An inclusive ramp model.** The detector ramp of HST/WFC3 is orbit dependent[19,20]. Standard procedures consist either of discarding the first orbit[9,18,19,31] or of fitting a different ramp for the first orbit[32]. We chose here to introduce a new ramp model to account for the time dependence of the ramp observed across the orbits of a visit (Fig. 1) and prevent systematically discarding the first orbit, which would otherwise reduce the observation baseline. (During the review process of this manuscript, such an approach was independently introduced in ref. [33]). As observed recently for HST/WFC3 observations of WASP-101 (ref. [20]), the variability of the detector ramp from one orbit to the next is enhanced when the electron ($e^-$) count per exposed pixel remains too low (<30,000$e^-$) to stabilize the charge-trapping effect during the first orbit. Therefore, the number of free-charge traps settles over multiple orbits to an equilibrium value driven by the charge-trapping rate and the charge-release rate. Because the probability of a photon-generated charge being trapped is directly proportional to the number of free-charge traps, both the timescale and the amplitude of the detector ramp settle as an exponential value whose own timescale, which is here larger than the duration of an orbit (~45 min), is proportional to the number of free traps. We therefore use the physically relevant following ramp model:

$$\frac{F_{\rm obs}(t)}{F(t)} = r_{\rm v}(t) r_{\rm o}(t) \quad (1)$$

$$r_{\rm v}(t) = \left(1 + a_1 {\rm e}^{-\frac{t}{a_2}}\right) \quad (2)$$

$$r_{\rm o}(t) = \left(1 + a_3 {\rm e}^{-\frac{t-t_{0_i}}{a_4 r_{\rm v}(t)}}\right) \quad (3)$$

where $r_{\rm v}(t)$ is the ramp induced by the progressive stabilization of the charge trapping, $r_{\rm o}(t)$ is the ramp induced by the charge-trapping effect (the 'traditional ramp'), $F_{\rm obs}(t)$ is the observed flux, $F(t)$ is the incoming flux, $t$ is the time from the first exposure of the visit, $t_{0_i}$ is the time of the first exposure of the $i$th orbit, which contains the exposure obtained at $t$, and $\{a_1, a_2, a_3, a_4\}$ are the model parameters.

Our model requires the same number of parameters as does fitting for a different ramp for the first orbit, while being physically relevant and accounting for the orbit dependence of the detector ramp. We find that our model combined with a second-order polynomial in time over each visit is strongly favoured (difference in the Bayesian information criterion is greater than or equal to −25). Supplementary Fig. 4 shows the best fits for visit 1 using our ramp model and different traditional ramps for the first orbit and the subsequent ones.

**HST/WFC3 spectroscopy.** The spectroscopic light curves are created for ten 0.05 μm bins from 1.15 μm to 1.65 μm (Supplementary Fig. 5). Of the 23 orbits obtained in this programme, two were substantially affected by the SAA as they started during the crossing (implying a high level of cosmic ray hits) and continued in GYRO mode (implying a large spectral drift). Both of these orbits occurred during a planetary transit: orbit 2 of visit 3 during a transit of planet d, and orbit 5 of visit 4 during a transit of planet g. This, therefore, prevented us from capitalizing on the repeated observations for both planets to reach a higher precision. As we observed hints of offsets in the absolute transit depths of planets e and f, we extracted their transmission spectra jointly from, respectively, visits 2 and 4 and visits 1 and 3 while allowing for an absolute transit depth offset from one visit to the next. Performing joint analyses allows us to further disentangle the visit-independent planetary signal from the visit-dependent systematics. Furthermore, it is a statistically more adequate approach than combining spectral estimates derived from individual visits in the context of systematics (red noise). We used the wavelength-dependent limb-darkening coefficients and analysis procedure (least-squares minimization fitting implementation to marginalize across a grid of systematic models, followed by adaptive Markov chain Monte Carlo implementations to sample the parameter posterior probability distributions) introduced in ref. [9]. Doing so, we achieved for visits 1–4 an average SDNR of 545 ppm, 526 ppm, 493 ppm and 494 ppm across all spectroscopic light curves in each visit, respectively.

**Uncertainty estimates in the flux measurements.** We estimate the uncertainty on the flux measurements from the standard deviation of the residuals of each individual orbit while accounting for a potentially reduced value due to the small sample size related to each orbit (up to 17 measurements). To do so, we prevent the uncertainty estimates being lower than the programme average outside the SAA crossing (220 ppm and 520 ppm for the white and coloured light curves, respectively). This approach allows the routine automatically to account for the larger SDNR of the early-SAA-crossing orbits (see Fig. 1).

**Atmospheric analysis.** We compared the derived transmission spectra of TRAPPIST-1 d, e, f and g with synthetic spectra representative of hydrogen-dominated atmospheres (Fig. 2) like those of the Solar System giant planets. We simulated the synthetic spectra following ref. [9] using the model introduced in ref. [34]. We used the atmospheric compositions of the 'mini-Neptune' (atmospheric mean molecular weigh $\mu = 2.6$ AMU) and 'Halley world' ($\mu = 14.9$ AMU) scenarios introduced in ref. [35] to simulate the hydrogen-dominated and water-dominated atmospheres, respectively. We used a 2% abundance for methane ($CH_4$) as the trace gas for the hydrogen-dominated atmosphere (similarly in the 'mini-Neptune' case, featuring water as the trace gas). We used an atmosphere with 80% carbon

dioxide, 13% methane, 3% nitrogen, 2% water and 2% hydrogen for the carbon-dioxide-rich atmosphere. We used for each planet the same mixing ratios and assume conservatively isocompositional and isothermal atmospheres in hydrostatic equilibrium. We used temperatures equal to the planets' equilibrium temperature assuming a 0.3 Bond albedo (265 K, 235 K, 200 K and 180 K for planets d, e, f and g, respectively).

For the planetary masses, we conservatively use the maximum masses that would allow each of the planets to harbour hydrogen-dominated atmospheres (hydrogen–helium envelopes greater than 0.01% of their total masses given their radii[36]). These masses are referenced as 'conservative' because they minimize the atmospheric scale height, the amplitude of the atmospheric signal in transmission and, thus, also the significance level to which the synthetic scenarios can be ruled out by the measured spectra. These theoretical upper limits correspond to $0.4\,M_{\oplus}$, $0.8\,M_{\oplus}$, $1\,M_{\oplus}$ and $1.15\,M_{\oplus}$, where $M_{\oplus}$ is the mass of Earth, for planets d, e, f and g, respectively. With this theory-based approach, our conclusions are thus also independent from the current mass estimates, which once refined could be used to derive quantitative atmospheric constraints.

**Code availability.** Conversion of the universal times for the photometric measurements to the barycentric Julian date/barycentric dynamical time system was performed using the online program created by J. Eastman and distributed at http://astroutils.astronomy.ohio-state.edu/time/utc2bjd.html. We have opted not to make available the codes used for the data extraction because they are currently an important asset of the researchers' tool kits. However, subproducts of the data extractions, such as corrected frames and extracted white and coloured light curves, can be found on the Mikulski Archive for Space Telescopes archive (http://archive.stsci.edu). For the same reason, we have opted not to make available all but one of the codes used for the data analyses. The Markov chain Monte Carlo software used by M.G. to analyse independently the photometric data is a custom Fortran 90 code that can be obtained from the corresponding author upon request.

**Data availability.** The data that support the plots within this paper and other findings of this study are available at the Mikulski Archive for Space Telescopes (https://mast.stsci.edu/portal/Mashup/Clients/Mast/Portal.html?searchQuery=trappist-1) and/or from the corresponding author upon reasonable request.

Received: 8 February 2017; Accepted: 20 December 2017;
Published online: 05 February 2018

## References

1. Gillon, M. et al. Seven temperate terrestrial planets around the nearby ultracool dwarf star TRAPPIST-1. *Nature* **542**, 456–460 (2017).
2. Gillon, M. et al. Temperate Earth-sized planets transiting a nearby ultracool dwarf star. *Nature* **533**, 221–224 (2016).
3. Owen, J. E. & Wu, Y. Kepler planets: a tale of evaporation. *Astrophys. J.* **775**, 105 (2013).
4. Jin, S. et al. Planetary population synthesis coupled with atmospheric escape: a statistical view of evaporation. *Astrophys. J.* **795**, 65 (2014).
5. Luger, R. & Barnes, R. Extreme water loss and abiotic $O_2$ buildup on planets throughout the habitable zones of M dwarfs. *Astrobiology* **15**, 119–143 (2015).
6. Owen, J. E. & Mohanty, S. Habitability of terrestrial-mass planets in the HZ of M dwarfs—I. H/He-dominated atmospheres. *Mon. Not. R. Astron. Soc.* **459**, 4088–4108 (2016).
7. Sagan, C. Reducing greenhouses and the temperature history of Earth and Mars. *Nature* **269**, 224 (1977).
8. Pierrehumbert, R. & Gaidos, E. Hydrogen greenhouse planets beyond the habitable zone. *Astrophys. J.* **734**, L13 (2011).
9. de Wit, J. et al. A combined transmission spectrum of the Earth-sized exoplanets TRAPPIST-1 b and c. *Nature* **537**, 69–72 (2016).
10. Bolmont, E. et al. Water loss from terrestrial planets orbiting ultracool dwarfs: implications for the planets of TRAPPIST-1. *Mon. Not. R. Astron. Soc.* **464**, 3728 (2016).
11. Bourrier, V. et al. Temporal evolution of the high-energy irradiation and water content of TRAPPIST-1 exoplanets. *Astron. J.* **154**, 121 (2017).
12. Kasting, J. F., Whitmire, D. P. & Reynolds, R. T. Habitable zones around main sequence stars. *Icarus* **101**, 108–128 (1993).
13. Zsom, A., Seager, S., de Wit, J. & Stamenkovic, V. Towards the minimum inner edge distance of the habitable zone. *Astrophys. J.* **778**, 109 (2013).
14. Kopparapu, R. k. et al. The inner edge of the habitable zone for synchronously rotating planets around low-mass stars using general circulation models. *Astrophys. J.* **819**, 84 (2016).
15. Hu, R. et al. Photochemistry in terrestrial exoplanet atmospheres. III. Photochemistry and thermochemistry in thick atmospheres on super Earths and mini Neptunes. *Astrophys. J.* **784**, 63 (2014).
16. Morley, C. V. et al. Thermal emission and reflected light spectra of super Earths with flat transmission spectra. *Astrophys. J.* **815**, 110 (2015).
17. Deming, D. et al. Infrared transmission spectroscopy of the exoplanets HD 209458b and XO-1b using the Wide Field Camera-3 on the Hubble Space Telescope. *Astrophys. J.* **774**, 95 (2013).
18. Kreidberg, L. et al. Clouds in the atmosphere of the super-Earth exoplanet GJ1214b. *Nature* **505**, 69–72 (2014).
19. Wakeford, H. R., Sing, D. K., Evans, T., Deming, D. & Mandell, A. Marginalizing instrument systematics in HST WFC3 transit light curves. *Astrophys. J.* **819**, 10 (2016).
20. Wakeford, H. R. et al. HST PanCET program: a cloudy atmosphere for the promising JWST target WASP-101b. *Astrophys. J.* **835**, L12 (2017).
21. Gillon, M. et al. The TRAPPIST survey of southern transiting planets. I. Thirty eclipses of the ultra-short period planet WASP-43 b. *Astron. Astrophys.* **542**, A4 (2012).
22. Demory, B.-O. et al. Hubble Space Telescope search for the transit of the Earth-mass exoplanet α Centauri B b. *Mon. Not. R. Astron. Soc.* **450**, 2043–2051 (2015).
23. Leconte, J., Forget, F. & Lammer, H. On the (anticipated) diversity of terrestrial planet atmospheres. *Exp. Astron.* **40**, 449–467 (2015).
24. Sing, D. K. et al. A continuum from clear to cloudy hot-Jupiter exoplanets without primordial water depletion. *Nature* **529**, 59–62 (2016).
25. Wakeford, H. R. & Sing, D. K. Transmission spectral properties of clouds for hot Jupiter exoplanets. *Astron. Astrophys.* **573**, A122 (2015).
26. Barstow, J. K. & Irwin, P. G. J. Habitable worlds with JWST: transit spectroscopy of the TRAPPIST-1 system? *Mon. Not. R. Astron. Soc.* **461**, L92–L96 (2016).
27. Morley, C. V., Kreidberg, L., Rustamkulov, Z., Robinson, T. & Fortney, J. J. Observing the atmospheres of known temperate Earth-sized planets with JWST. *Astrophys. J.* **850**, 121 (2017).
28. Zsom, A. A population-based habitable zone perspective. *Astrophys. J.* **813**, 9 (2015).
29. McCullough, P. & MacKenty, J. *Considerations for Using Spatial Scans with WFC3* Instrument Science Report WFC3 2012-08 (Space Telescope Science Institute, Baltimore, 2012).
30. Knutson, H. A. et al. Hubble Space Telescope near-IR transmission spectroscopy of the super-Earth HD 97658b. *Astrophys. J.* **794**, 155 (2014).
31. Berta, Z. K. et al. The flat transmission spectrum of the super-Earth GJ1214b from Wide Field Camera 3 on the Hubble Space Telescope. *Astrophys. J.* **747**, 35 (2012).
32. Line, M. R. et al. No thermal inversion and a solar water abundance for the hot Jupiter HD 209458b from HST/WFC3 spectroscopy. *Astron. J.* **152**, 203 (2016).
33. Zhou, Y. et al. A physical model-based correction for charge traps in the Hubble Space Telescope's Wide Field Camera 3 near-IR detector and its applications to transiting exoplanets and brown dwarfs. *Astron. J.* **153**, 243 (2017).
34. de Wit, J. & Seager, S. Constraining exoplanet mass from transmission spectroscopy. *Science* **342**, 1473–1477 (2013).
35. Benneke, B. & Seager, S. Atmospheric retrieval for super-Earths: uniquely constraining the atmospheric composition with transmission spectroscopy. *Astrophys. J.* **753**, 100 (2012).
36. Howe, A. R., Burrows, A. & Verne, W. Mass-radius relations and core-envelope decompositions of super-Earths and sub-Neptunes. *Astrophys. J.* **787**, 173 (2014).

## Acknowledgements

This work is based on observations made with the NASA (National Aeronautics and Space Administration)/European Space Agency HST that were obtained at the Space Telescope Science Institute, which is operated by the Association of Universities for Research in Astronomy. These observations are associated with programme GO-14873 (principal investigator J.d.W.), support for which was provided by NASA through a grant from the Space Telescope Science Institute. H.R.W. acknowledges funding from the European Research Council (ERC) under the European Union's Seventh Framework Programme (FP7/2007–2013)/ERC grant agreement no. 336792, and funding under the Space Telescope Science Institute Giacconi Fellowship. This work was partially conducted while on appointment to the NASA Postdoctoral Program at Goddard Space Flight Center, administered by the Universities Space Research Association through a contract with NASA. L.D. acknowledges support from the Gruber Foundation Fellowship. E.J. and M.G. are Research Associates at the Belgian Fonds (National) de la Recherche Scientifique (FRS-FNRS). The research leading to these results has received funding from the ERC under the FP/2007–2013 ERC grant agreement no. 336480, and from a grant from the Concerted Research Actions, financed by the Wallonia-Brussels Federation. B.-O.D. acknowledges support from the Swiss National Science Foundation (PP00P2–163967). This work was also partially supported by a grant from the Simons Foundation (PI Queloz, grant no. 327127). This project has received funding from the ERC under the European Union's Horizon 2020 research and innovation programme (grant agreement no. 679030/WHIPLASH). V.B. acknowledges the financial support

of the Swiss National Science Foundation. We thank D. Taylor, K. Stevenson, N. Reid and K. Sembach for their assistance in the planning, execution and/or analysis of our observations. J.d.W., H.R.W. and N.K.L. thank also the Howards-Lewis Team and F. Dory for their support and contributions during the data-processing phase of this work.

## Author contributions

J.d.W. and N.K.L. led the management of the survey. J.d.W. planned the observations. J.d.W and H.R.W. led the data reduction and analysis with the support of N.K.L., L.D., M.G. and B.-O.D. J.d.W. led the data interpretation with the support of H.R.W., N.K.L., V.S., J.L., J.E.O. and F.S. Every author contributed to the writing of the manuscript and/or the HST proposal behind these observations.

## Competing interests

The authors declare no competing financial interests.

## Additional information

**Supplementary information** is available for this paper at https://doi.org/10.1038/s41550-017-0374-z.

**Reprints and permissions information** is available at www.nature.com/reprints.

**Correspondence and requests for materials** should be addressed to J.d.

**Publisher's note:** Springer Nature remains neutral with regard to jurisdictional claims in published maps and institutional affiliations.